Topological Flow Structures in a Mathematical Model for Rotation-Mediated Cell Aggregation

Alexander Wiebel[1], Raymond Chan[2], Christina Wolf[3], Andrea Robitzki[3], Angela Stevens[4], and Gerik Scheuermann[5]

[1] Max-Planck-Institut für Kognitions- und Neurowissenschaften, Stephanstraße 1A, 04103 Leipzig, Germany, wiebel@cbs.mpg.de

[2] Max-Planck-Institut für Mathematik in den Naturwissenschaften, Inselstraße 22, 04103 Leipzig, Germany, rchan@mis.mpg.de,

[3] Universität Leipzig, Center for Biotechnology and Biomedicine (BBZ), Abteilung Molecular biological-biochemical Processing Technology, Deutscher Platz 5, 04103 Leipzig, Germany, andrea.robitzki@bbz.uni-leipzig.de, christina.wolf@bbz.uni-leipzig.de,

[4] Universität Heidelberg, Angewandte Mathematik und Bioquant, Im Neuenheimer Feld 267, 69120 Heidelberg, Germany angela.stevens@uni-hd.de

[5] Universität Leipzig, Abteilung Bild- und Signalverarbeitung, PF 100920, 04009 Leipzig, Germany, scheuer@informatik.uni-leipzig.de

Abstract. In this paper we apply vector field topology methods to a mathematical model for the fluid dynamics of reaggregation processes in tissue engineering. The experimental background are dispersed embryonic retinal cells, which reaggregate in a rotation culture on a gyratory shaker, according to defined rotation and culture conditions. Under optimal conditions, finally complex 3D spheres result. In order to optimize high throughput drug testing systems of biological cell and tissue models, a major aim is to understand the role which the fluid dynamics plays in this process. To allow for a mathematical analysis, an experimental model system was set up, using micro-beads instead of spheres within the culture dish. The qualitative behavior of this artificial model was monitored in time by using a camera. For this experimental setup a mathematical model for the bead-fluid dynamics was derived, analyzed and simulated. The simulations showed that the beads form distinctive clusters in a layer close to the bottom of the petri dish. To analyze these patterns further, we perform a topological analysis of the velocity field within this layer of the fluid. We find that traditional two-dimensional visualization techniques like path lines, streak lines and current time-dependent topology approaches are not able to answer the posed questions, for example they do not allow to find the location of clusters. We discuss the problems of these techniques and develop a new approach that measures the density of advected particles in the flow to find the moving point of particle aggregation. Using the density field the path of the moving aggregation point is extracted.

1 Introduction

The topology of two-dimensional time-dependent vector fields has been an active field of research in recent years [7, 18, 17]. In this paper we investigate the features of a mathematical model for the fluid flow of a mixture of beads and growth medium in a layer close to the bottom of a petri dish, which rotates on a gyratory shaker. A moving zero in the instantaneous vector field is the most striking feature of the flow. This suggests the application of topological methods for the desired analysis. To provide the basis for the discussion of the vector field we will first describe the experiment, the mathematical model and its simulation, which leads to the vector field.

2 The Experiment, the Mathematical Model and its Simulation

The biological experiment, which builds the background for the mathematical model, its simulation, visualization and visualization techniques, investigates rotational tissue cultures, which are relevant for high throughput drug testing systems in regenerative medicine. A petri dish, which contains growth medium and dispersed embryonic cells, is located on a gyratory shaker. The specificities of the rotation affect the fluid flow in the petri dish and thus the motion of the cells. Without any movement of the petri dish, the cells generally form a mono-layer at the bottom and grow in a disorganized manner. However, under a specific rotation of the petri dish, the cells finally form several 3D spheroids. Details about these methods and further results can be found in [9, 8, 10].

To understand the role the fluid dynamics play in this reaggregation and structure forming process, an experimental model system was set up. Microscopic beads were put into the culture dish and rotated under the same conditions as the cell systems. This system is assumed to serve well as a model system for the cell-based fluid dynamics under consideration. In the experiment clustering of the beads was observed for a rotation speed of 70RPM but not for a rotation speed of 60RPM. Further interesting patterns and phase transitions occurred. To confirm the hypothesis that *mechanical* aggregation plays a key role in the initial clustering of the beads, a mathematical model for the fluid dynamics was derived and numerically analyzed. The basis of the mathematical model are the incompressible Navier-Stokes Equations, which are solved in a domain representing the petri dish. Fictitious body forces, acting on the fluid, are added. These result from the rotation of the petri dish. A dimensional analysis was performed and by regular perturbation techniques the model was reduced to a shallow water type of problem. The main assumption is, that the Reynolds number in horizontal direction is much larger than the Reynolds number in vertical direction. For the numerical discretization a finite volume method was employed, which takes into account that the flow is mainly laminar. The qualitative behavior of the mathematical model compares well to the aggregation behavior of the beads observed in the experiment. Clusters of particles are found to rotate around the center

of the petri dish. Further details on the mathematical model, its simulation and first visualizations are given in [3]. The simulations of this model provide the data, which are analyzed in the following.

To justify our use of two-dimensional visualization techniques it should be noted that the beads (in the rest of the paper often called *the particles*) are expected to stay in a layer close to the bottom of the petri dish. The particles are only expected to leave this layer at singular points in the flow.

3 Related Work in Vector Field Topology Visualization

As mentioned, topological methods seem to be a good choice for the visualization of the presented application. Of particular relevance for the present work are techniques that permit to track the continuous evolution of the topology as it evolves over time. Improving on a scheme introduced by Helman and Hesselink [7], which graphically reconnects the topological skeletons extracted in successive time steps, Tricoche *et al.* [18] proposed a scheme that computes the continuous path followed by two-dimensional *singularities* (where the flow velocity vanishes) across the space-time domain. Their approach explicitly characterizes bifurcations, which correspond to critical changes affecting the structure of the topological skeleton. An alternative method that extracts the topological evolution by means of numerical integration over the space-time continuum was introduced by Theisel *et al.* [16]. Extensions to three-dimensional transient flows have been presented for both methods [5, 15]. Just recently Wiebel *et al.* [19] introduced a technique allowing to track singularities on curved surfaces by using parameterizations in combination with the existing two-dimensional techniques.

A first approach to time-dependent topology not using streamlines, called path line oriented topology, was undertaken by Theisel *et al.* [17]. They distinguish sectors of attracting, repelling and saddle-like behavior of the path lines. This is different from the usual concept of topology, which is to observe how trajectories behave under an integration *until infinity* while their method only considers local properties of the path lines. They call this approach topological because it also aims at segmenting the domain into areas of different flow behavior. To be able to apply an asymptotic analysis for path lines Shi *et al.* [14] restrict themselves to periodic fields and present a path line oriented topology for periodic 2D time-dependent vector fields. Unfortunately, this approach is not applicable in our case as the flow considered in this paper is not periodic.

4 Application of Common Visualization Techniques

In this section we describe the application of a number of standard visualization techniques to the petri dish flow field. We describe the different viewpoints taken by these techniques and show their deficiency to illustrate certain features of the flow. This will promote the need for the new technique developed in Section 5.

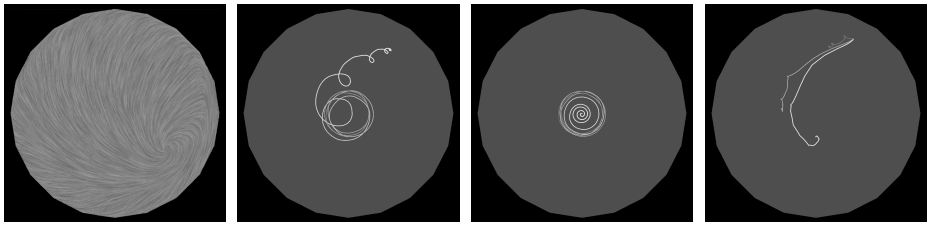

(a) LIC of instantaneous vector field for $t = 37$. Note the sink in the right part.

(b) Path line from outer area.

(c) Path line from center.

(d) Streak lines started at $t = 2$ shown for $t \in \{25, 37, 79\}$.

Fig. 1. Application of different standard visualization techniques for vector fields.

4.1 Streamlines

Streamlines and their dense counterpart the line integral convolution [2] (LIC) are the most frequently used visualization techniques for flow fields. As they only illustrate the momentary direction of a flow, animations are often used for time-dependent fields. For the current application such an animation only shows the overall rotation behavior and the existence of an attracting singularity in the flow (see Figure 1(a)). The information about the long-term behavior of particles given by this visualization is very small. A more detailed discussion of the attracting singularity will be given in the section about streamline oriented topology (Section 4.4).

4.2 Path Lines

As path lines reflect the path of a particles they should be better suited for finding the path of the moving agglomeration. Indeed, the path lines shown in Figures 1(b) and 1(c) (coming from the border respectively the center of the domain) show that the particles approach a kind of common cyclic structure. A naive interpretation of this cyclic structure could be that the particles are distributed around the circle and form a kind of ring. It does not become clear that the particles tend to agglomerate around one position and that this agglomeration moves on the displayed circle (see Figures 2(b) and 2(c)).

4.3 Streak Lines

Well known from physical flow experiments, streak lines seem to be a good standard choice to investigate the two-dimensional flow field. Most images produced by streak lines seem to yield a good representation of the underlying flow. Good examples can be found in a paper by Sheard *et al.* [13] and many other papers in the same journal as well as in a book by Batchelor [1]. However, it is also known that care has to be taken with the interpretation of streak lines [6]. Representative streak lines for our example are shown in Figure 1(d). The image is

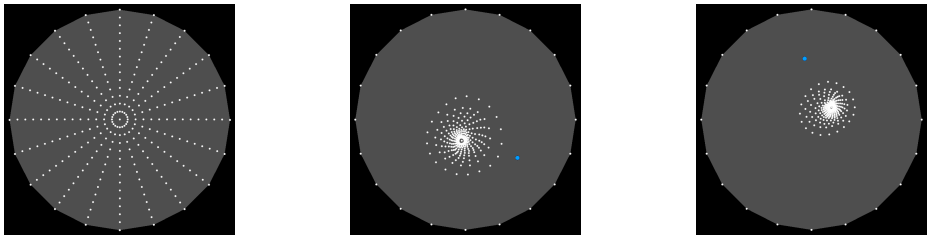

(a) (b) (c)

Fig. 2. Particles traced in the rotating flow show that the point attracting the particles is not the singularity moving through the flow. (a) Particles (white) at $t = 1$. (b) Particles after advection until $t = 37$ with attracting singularity (blue) at $t = 37$. Compare the position of the singularity to LIC in Figure 1(a). (c) Particles after advection until $t = 40$ with attracting singularity at $t = 40$.

only able to illustrate the fact that the particles come closer to the center of the dataset with longer advection time. An animation over a certain time interval shows the general rotation but does not reveal any salient features either.

4.4 Streamline Oriented Topology

The best candidates for showing the aggregation of the particles seem to be topological methods as they can track the path of attracting singularities (also known as *sinks*) through time. Naively, one would expect that the particles at a certain point of time tend to agglomerate at the momentary position of the sinks. In our example we have exactly one such sink and thus would expect the particles to converge to this point.

To inspect these presumptions we traced the particles shown in Figure 2(a) a certain amount of time t and computed the singularity of the instantaneous vector field at time t. Figures 2(b) and 2(c) show the resulting images. The images clearly contradict the presumptions. The particle agglomeration is not located around the singularity, it rather lags approximately one third of a rotation period behind the zero of the vector field. A possible explanation for the difference between the point of aggregation and the singularity might be that the singularity lies in a large area with nearly zero vectors. Thus the concentration process can not (or only very slowly) appear there. It is probably much stronger in areas with vectors of large magnitude. Additionally, even a significantly moving and strongly attracting singularity would not be able to drag the agglomeration along its path because vectors on opposite sides of the singularity point in opposite directions. The particles thus are moved in one direction before the singularity passes (close to) their position and in the opposite direction thereafter.

As our example shows, there are probably only few cases for which a singularity in time-dependent flow has an interesting meaning. One of these few cases is a singularity on a surface that indicates separation of the flow from the surface (see e.g. [19]).

4.5 Path Line Oriented Topology

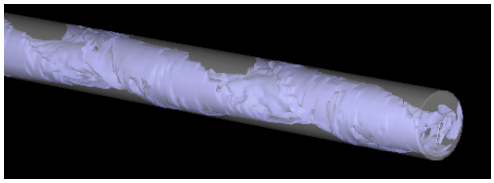

(a) Path line oriented topology in complete time-dependent field. Third dimension used to stack time steps ($60 < t < 80$ visible). Isosurface encloses attracting behavior.

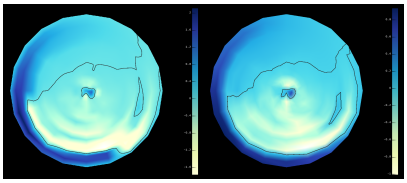

(b) Path line oriented topology (left) compared to divergence (right) for $t = 70$. Colormap and zero isolines divide the field into areas with converging (negative values) and diverging behavior (positive values)

Fig. 3. Path line oriented topology.

As discussed in Section 4.2, path lines are more effective for illustrating the time-dependent nature of the flow than streamlines. Thus it is worth looking at the visualization yielded by the so-called path line oriented topology as introduced by Theisel *et al.* [17]. Although, this approach does not really compute path lines and analyze their behavior it still classifies the local time-dependent behavior as saddle-like, attracting (converging) or repelling (diverging).

The application of path line oriented topology to our data reveals no areas of saddle-like behavior. The domain is only divided into attracting and repelling parts. Figure 3(a) shows the attracting parts enclosed by an isosurface. It is apparent that not only specific points are marked as attracting but large areas. Thus, the approach does not identify the features we are searching for, i.e. points of particle attraction. It only illustrates that the attracting and repelling parts revolve around the center of the dish over time.

Figure 3(b) shows a comparison of one of the characteristic fields of the path line oriented topology (here sum of eigenvalues) and the divergence of the instantaneous vector field. Both images illustrate the behavior at $t = 70$. The comparison makes a strong statement about the meaning of the path line oriented topology for our data. It seems that the areas marked as attracting or repelling closely correspond to areas of negative or positive divergence. This is interesting because the computation of path line oriented topology is much more time consuming than the computation of divergence.

4.6 FTLE

As we are searching for converging particles, one might suggest to use FTLE (Finite-Time Lyapunov Exponent) fields for visualization (see e.g. [4, 11]). Our experiments, however, showed that while FTLE is able to characterize the time-dependent convergence better than path line oriented topology does, it does not identify the point of attraction either. Figure 4 shows a color mapping of FTLE^{-}

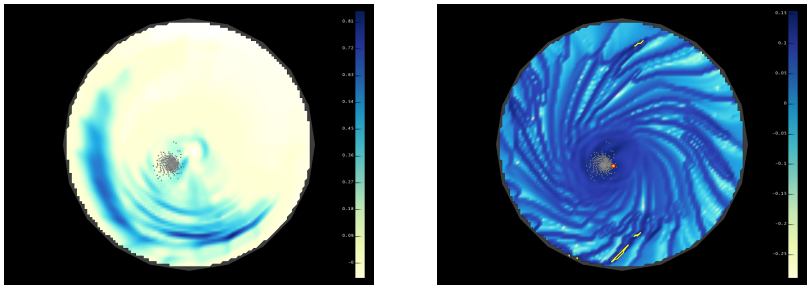

Fig. 4. FTLE$^-$ with particle cluster for $t = 70$. Integration for 1 (left) and 20 time units (right). Very high magnitude of FTLE$^-$ marked yellow. Note the small (enlarged) yellow point fairly close to the particles.

(i.e. FTLE using backward integration) for $t = 70$ together with a particle cluster at the same instant. The left image results from a very short integration and does not help us, as the FTLE is dominated by interpolation artifacts resulting from the coarse grid. This influence vanishes for longer integration times (right image). But even in this image the center of the particles can not be determined correctly as strong FTLE$^-$ can be found in a large area around the particles. Taking the maximum does not help as there are several very large values (marked yellow), none of which represents the center correctly. The relatively "noisy" FTLE field (right image) results from the fact that many particles leave the domain during long-time backward integration.

5 Detection of Point of Attraction

In the previous section we have shown that popular existing visualization techniques for unsteady two-dimensional flow fields, while being able to give hints as to where particles converge, are not capable of finding the point of aggregation of the particles. In the rest of the current section we will describe a new approach specially designed to find and track the point of particle aggregation.

5.1 Idea

The basis for the presented technique is the following observation: Particles started at earlier times, in general, can be found in the convex hull of particles started at later time steps (see Figure 5(b)). This means that the point of the largest particle density is the point that is attracting particles. So the main procedure of the proposed technique is the following: We trace particles from a grid at a number of time steps before the observation time. We then compute the density of the particles and extract maxima of this density. The maxima show us the positions of the points of particle attraction. As these points move over time we repeat the procedure for several observation times. Connecting the points of the different observation times yields the path of a point of attraction.

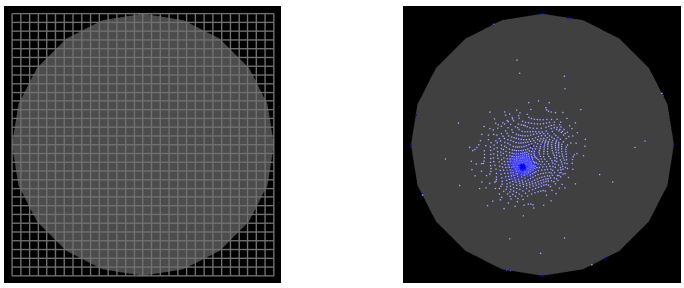

(a) (b)

Fig. 5. Particle advection for density computation. (a) Regular grid for starting particles. (b) Particles started at earlier time steps lie in convex hull of particles from later times (except points started and remaining exactly on the boundary). Points color coded by starting time.

5.2 Seeding of Particles

The first step of the technique is seeding the particles for the advection. Care has to be taken because the initial distribution influences the density of the particles after advection. As can be seen from the initial particle positions in Figure 2(a), the grid of the simulation is a structured radial grid. Particles seeded on this grid have a non-uniform density, i.e. a higher density near the center. Figure 2(b) shows that the non-uniformity of the initial distribution is still visible after particle advection. This can cause the existence of density maxima (resulting from initially high density) at points where advection has not increased density. This, again, can make finding the correct point of attraction impossible.

Consequently, we need a uniform density at the beginning. A simple distribution fulfilling this constraint can be obtained by seeding the particles at the points of regular grid as shown in Figure 5(a). For starting particles at different time steps we choose the seeding grids to be equidistant in time.

5.3 Density Computation

We store the density on a second regular grid. It may have a different resolution than the one used for seeding the particles. For every point of the density grid we simply count the particles that are closer to this point than to any other. This is equivalent to counting the particles in all cells of the dual of the density grid. Since the grid is regular, each cell of the dual grid is defined by two intervals on the two coordinate axes. Knowing the resolution and the bounding box of the grid, it is easy to compute the intervals and thus the grid position each particle position belongs to. We increment the particle count of the density grid position we have found a particle to be closest to and repeat this for all particles and starting times to obtain the desired density field. Examples of density fields for our data set are shown in Figure 6.

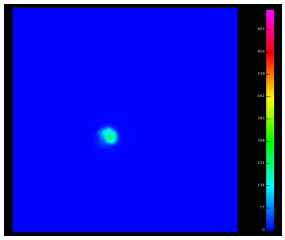

(a) Density of particles traced from one grid at $t = 50$.

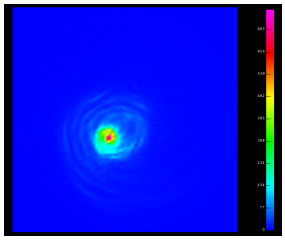

(b) Density of particles traced from ten grids at $t = 50, 52, \ldots, 68$.

Fig. 6. Color coded density distribution for time $t = 70$ and resolution of 100×100. The length and with of the square are two times the radius of the petri dish.

5.4 Extraction of Density Maxima

The density field computed in the previous step is given on the points of the density grid. Usually one introduces a certain interpolation scheme to have continuous data over the whole domain. If the underlying grid consists of simplices, i.e. triangles in the two-dimensional case, one often uses a linear interpolation. Inside quadrangular cells bilinear interpolation is commonly used. For both interpolation schemes maxima and minima can only exist at vertices. Thus, their detection is straight forward. Using the connectivity induced by the grid we simply compare the value at each vertex with all directly adjacent vertices. If all adjacent vertices have smaller values than the considered vertex a maximum has been found. If only the global maximum is of interest we simply run through all positions and store the position of the largest value. In order to eliminate insignificant maxima and merge very close maxima, a low pass filter can be applied. This was not necessary for the presented data set. The only significant maximum in the petri dish flow at $t = 70$ is clearly visible in Figure 6.

5.5 Tracking of Density Maxima

So far only the positions of the maxima in the different time steps have been determined. These are the positions of the point of attraction at different times. To extract the complete path of the moving point we have to connect the positions of corresponding maxima between the time steps. In our case, where we have only one important maximum, we simply connect the positions by straight lines. Images of the tracked maximum are shown in Figure 7. As the maxima can only appear at vertices of the grid underlying the density field, the smoothness of extracted paths strongly depends on the resolution of this grid. A second influencing factor is the distance of the density fields in time. This is why the paths in the figure are relatively jaggy. The paths in Figure 7 cover only relatively short time spans to avoid visual clutter by crossing and overlapping.

(a) Attraction path consisting of 50 observations with density field resolution 100×100 and seeding resolution 30×30

(b) Attraction path consisting of 30 observations with density field resolution 40×40 and seeding resolution 10×10.

Fig. 7. Attraction path for $72 < t < 80$ extracted by tracing from $t - 20$. Smoothness of path depends on resolution of density field and number of observations. Different colored particles for different observation times t (traced from $t - 15$) provide context.

Multiple Maxima As mentioned, we connect the single maximum in our data from one time step to the next. When aiming at tracking several maxima in one density field over time, more elaborate techniques are needed. Several methods for tracking features in scalar fields can be found in the literature, see e.g. [12].

5.6 Performance, Discussion and Acceleration

The computation times for the paths strongly depend on the resolution of the seeding grid, the number of observations and the number of grids used to seed the particles for each observation. In Figure 7 they range from 4 minutes for the path in Figure 7(b) to one hour for the path in Figure 7(a).

Increasing the resolution of the density grid increases the computation time only marginally. This is why we chose the density resolution to be different from the seeding resolution. It allows us to increase the precision of the detected maximum position at nearly no cost. However, it is important to note that the density resolution can not be chosen completely independent from the seeding resolution. If the resolution difference becomes to large, the number of particles becomes insufficient to produce a reasonable density field. The result are many positions with one or two particles closest to them and no position being a significant maximum. This renders the extracted paths meaningless. We found density resolutions below 5 times the seeding resolution to yield good results.

The large number of particle advections is the dominating factor of the computation time. There is a large potential for acceleration. The most obvious acceleration is parallelizing the particle advection. This yields a computation time nearly inverse proportional to the number of tasks processable in parallel.

A second idea, more specific to the presented approach, is to reuse previously traced particles. This idea is applicable if we do not only compute the position for a single time but perform a tracking of the position through a number of time

steps. Let $t_0^a < t_1^a < \ldots < t_n^a$ be equidistant times for which particles have been traced until $t^a = t_n^a$. Define $t_0^b < t_1^b < \ldots < t_n^b$ analogously. Let $t^a < t^b$. If we now store all positions of all particles traced for t^a in groups depending on their start time t_i^a we can reuse the particles of all but one group (t_0^a) for computing the positions of the particles for t_i^b. Let the distance between two times be Δt. Then the positions of the particles starting at $t_0^b, \ldots, t_{n-1}^b$ and being observed at t^b can be computed by tracing the particles of the groups $t_1^a, \ldots, t_n^a$ for Δt. Obviously, this saves a large amount of computation time, as nearly all particles[1] observed at t^b need only to be traced for the relatively short time span Δt. Without this acceleration the mean time span traced is $\frac{n\Delta t}{2}$. Thus, reusing the previous particle positions we achieve an acceleration by a factor of approximately $\frac{n}{2}$.

6 Conclusion

We have discussed the application of several visualization techniques that are commonly used to illustrate two-dimensional time-dependent flow at a biofluid dynamic model. It turned out that all these existing techniques are not able to show the desired information or features of the vector field, i.e. the location of the point where particles tend to aggregate. Hence, a new technique computing the density of particles started at regularly distributed points at regularly spaced time steps is introduced. The density field obtained with this technique is then used to compute the desired location for any time step of interest. Thus, a curve representing the moving particle aggregation center can be defined. It is important to note that this curve is different from the path of the zero in the instantaneous velocity field.

We plan to improve our acceleration techniques to be able to extend our method to unsteady 3D vector fields where the computation time becomes even more crucial. Furthermore, we recommend the usage of our method only if the existence of an interesting point of aggregation is known, as otherwise a large number of false positives might corrupt the visualization. A method for detecting the existence of points of aggregation is needed.

Acknowledgments

We like to thank C. Garth for supplying his DOPRI5 code and W. Hackbusch, S. Luckhaus, and J.J.L. Velázquez for fruitful discussions on the mathematical model and the numerical code. During the course of this work A. Wiebel was supported by DFG grant SCHE 663/3-8 and hired by the BSV group at the University of Leipzig. R. Chan and C. Wolf were supported by the DFG Graduate College InterNeuro (GRK 1097) as well as A. Robitzki and A. Stevens as members and supervisors of this College. Further, A. Robitzki was supported by the DFG via SFB 610 - Z5. A. Stevens' work for this project was done, while she was hired by the Max-Planck-Institute for Mathematics in the Sciences, Leipzig.

[1] The particles of group t_n^b do not need to be traced. They are already at time t^b.

References

1. G. K. Batchelor. *An Introduction to Fluid Dynamics*. Cambridge University Press, 1967. Cambridge Mathematical Library Edition.
2. B. Cabral and L. C. Leedom. Imaging Vector Fields Using Line Integral Convolution. In *SIGGRAPH '93*, pages 263–270. ACM Press, 1993.
3. Raymond Chan. *A Biofluid Dynamic Model for Centrifugal Accelerated Cell Culture Systems*. PhD thesis, Fakultät für Mathematik und Informatik, Universität Leizig, DFG-Graduate College InterNeuro (GRK 1097), 2008. Preprint.
4. C. Garth, F. Gerhard, X. Tricoche, and H. Hagen. Efficient computation and visualization of coherent structures in fluid flow applications. *IEEE Transactions on Visualization and Computer Graphics*, 13(6):1464–1471, 2007.
5. C. Garth, X. Tricoche, and G. Scheuermann. Tracking of Vector Field Singularities in Unstructured 3D Time-Dependent Datasets. In *IEEE Visualization 2004*, pages 329 – 336. IEEE Computer Society, October 2004.
6. F. R. Hama. Streaklines in a perturbed shear flow. *PoF*, 5(6):644–650, June 1962.
7. J. L. Helman and L. Hesselink. Surface Representations of Two- and Three-Dimensional Fluid Flow Topology. In *IEEE Visualization '90*, pages 6–13. IEEE Computer Society Press, 1990.
8. P.G. Layer, A. Robitzki, A. Rothermel, and E. Willbold. Of layers and spheres: the reaggregate approach in tissue engineering. *Trends Neurosci.*, 25:131–134, 2002.
9. A. Mack and A. Robitzki. The key role of butyrylcholinesterase during neurogenesis and neural disorders: An antisense-5'-butyrylcholinesterase DNA study. *Prog. Neurobiol.*, 60:607–628, 2000.
10. A. Rothermel, T. Biedermann, W. Weigel, R. Kurz, M. Rüffer, P.G. Layer, and A. Robitzki. Artificial design of 3d retina-like tissue from dissociated cells of the mammalian retina by rotation-mediated cell aggregation. *Tissue Eng.*, 11(11-12):1749–1756, 2005.
11. F. Sadlo and R. Peikert. Efficient visualization of lagrangian coherent structures by filtered AMR ridge extraction. *IEEE TVCG*, 13(6):1456–1463, 2007.
12. Ravi Samtaney, Deborah Silver, Norman Zabusky, and Jim Cao. Visualizing Features and Tracking Their Evolution. *IEEE Computer*, 27(7):20 – 27, 1994.
13. G. J. Sheard, T. Leweke, M. C. Thompson, and K. Hourigan. Flow around an impulsively arrested circular cylinder. *Physics of Fluids*, 19(8), 2007.
14. Kuangyu Shi, Holger Theisel, Tino Weinkauf, Helwig Hauser, Hans-Christian Hege, and Hans-Peter Seidel. Path line oriented topology for periodic 2D time-dependent vector fields. In *Proc. EuroVis 2006*, pages 139–146, Lisbon, Portugal, May 2006.
15. H. Theisel, J. Sahner, T. Weinkauf, H.-C. Hege, and H.-P. Seidel. Extraction of Parallel Vector Surfaces in 3D Time-Dependent Fields and Application to Vortex Core Line Tracking. In *IEEE Visualization 2005*, pages 631–638, October 2005.
16. H. Theisel and H.-P. Seidel. Feature Flow Fields. In *VISSYM '03: Proc. of the Sym. on Data Visualisation 2003*, pages 141–148. Eurographics Association, 2003.
17. H. Theisel, T. Weinkauf, H.-C. Hege, and H.-P. Seidel. Topological methods for 2d time-dependent vector fields based on stream lines and path lines. *IEEE Transactions on Visualization and Computer Graphics*, 11(4):383–394, 2005.
18. Xavier Tricoche, Thomas Wischgoll, Gerik Scheuermann, and Hans Hagen. Topology Tracking for the Visualization of Time-Dependent Two-Dimensional Flows. *Computers & Graphics*, 26(2):249 – 257, 2002.
19. A. Wiebel, X. Tricoche, D. Schneider, H. Jänicke, and G. Scheuermann. Generalized streak lines: Analysis and visualization of boundary induced vortices. *IEEE TVCG*, 13(6):1735–1742, 2007.